Automatic Construction of Building Footprints from Airborne LIDAR Data

Keqi Zhang, Jianhua Yan, and Shu-Ching Chen, *Senior Member, IEEE,*

***Abstract*— This paper presents a framework that applies a series of algorithms to automatically extract building footprints from airborne LIDAR measurements. In the proposed framework, the ground and non-ground LIDAR measurements are first separated using a progressive morphological filter. Then, building measurements are identified from non-ground measurements using a region growing algorithm based on the plane-fitting technique. Finally, raw footprints for segmented building measurements are derived by connecting boundary points, and the raw footprints are further simplified and adjusted to remove noise caused by irregularly spaced LIDAR measurements. Data sets from urbanized areas including large institutional, commercial, and small residential buildings were employed to test the proposed framework. Quantitative analysis showed that the total of omission and commission errors for extracted footprints for both institutional and residential areas was about 12%. The results demonstrated that the proposed framework identified building footprints well.**

***Index Terms*— Airborne LIDAR, building footprint.**

I. Introduction

BUILDING footprints are one of the fundamental GIS data components that can be used to estimate energy demand, quality of life, urban population, and property taxes [1]. Accurate building footprint data are essential for construction of urban landscape models, assessment of urban heat island effect, and estimation of building base elevation for flood insurance [2]. In addition, footprint data in combination with height values can be used to generate three-dimensional (3D) building models for visualization in GIS. Traditionally, aerial photographs and high-resolution satellite images were the most effective data sources for extraction of building footprints. Manual derivation of building geometric data from a remote sensing image for a large area is cost prohibitive and time consuming. Therefore, numerous studies have been done to develop automated methods to extract footprints [3]-[6]. However, the success of the automated methods is limited due to the influence of sun shadow and relief displacement of high buildings in remote sensing images.

Recent emerging airborne light detection and ranging (LIDAR) technology provides a promising alternative for measuring buildings. Airborne LIDAR systems derive irregularly spaced 3D point measurements of objects, including ground, buildings, trees, and cars scanned by the laser beneath the aircraft. Compared to aerial photographs and satellite images, LIDAR measurements are not influenced by sun shadow and relief displacement. However, voluminous point data pose a new challenge for automated extraction of building information from LIDAR measurements because many raster image processing techniques cannot be directly applied to irregularly spaced points.

This paper presents algorithms for the extraction of building footprints from LIDAR measurements. The presented work is focused more on 2D footprint extraction than 3D building models. The paper is arranged as follows. Section II reviews the previous work. Section III describes the algorithms that derive building footprints. Section IV describes the sample LIDAR data set used by this study and parameters for data processing. Section V examines the results by applying footprint extraction algorithms to the sample data set and discusses several factors influencing footprint extraction algorithms. Section VI includes conclusions.

II. LITERATURE REVIEW

Two steps are involved in extracting a building footprint: identifying building measurements from LIDAR data and deriving the footprint polygon. Two ways are often utilized to identify building measurements from LIDAR data. One is to separate ground, buildings, trees, and other measurements from LIDAR data simultaneously [7][8]. The more popular way is to separate the ground from non-ground LIDAR measurements first and then identify the building points from non-ground measurements [9]-[11]. Numerous algorithms have been developed to identify ground measurements from LIDAR data [12]. The non-ground measurements can be derived by removing identified ground data from a raw data set. The critical step is to classify the building and vegetation points which dominate non-ground measurements.

Morgan and Tempfli [9] applied Laplacian and Sobel operators to height surfaces to separate building and tree measurements. Filin [8] and Morgan and Habib [13] separated building and tree measurements using the parameters for a plane which fits a LIDAR point and its neighbors within a local window. Elberink and Mass [14] segmented LIDAR data using anisotropic height texture measures. Alharthy and Bethel [15] employed the height difference between the first and last return measurements to distinguish building and tree measurements. The Hough Transform has also been used to identify building

Manuscript received June 27, 2005; revised February 23, 2006. This work was supported by the Florida Hurricane Alliance Research Program sponsored by National Oceanic and Atmospheric Administration and by the National Science Foundation under contract EAR-0518962.

K. Zhang is with the Department of Environmental Studies and International Hurricane Research Center, Florida International University, Miami, FL 33199 USA (e-mail: zhangk@ fiu.edu).

J. Yan and S.-C. Chen are with the Distributed Multimedia Information System Laboratory, School of Computing and Information Sciences, Florida International University, Miami, FL 33199 USA (e-mail: jyan001@ cs.fiu.edu; chens@cs.fiu.edu;).

points from non-ground measurements [11] or directly from raw LIDAR data [16][17].

However, these methods suffer from various problems. For example, the height differences from first and last returns do not work for areas covered by dense trees where laser pulses cannot penetrate. It is difficult to define an optimum voting size in the parameter space for the Hough Transform because local height changes of building roof surfaces are varied. The region growing algorithm is often employed to identify building points in a method that uses estimated plane parameters for a point and its neighbors. The processes of region growing are variable, depending on the selection of seed points. The effect of selecting seed points on segmentation results has not been examined.

After measurements for a building are identified, a raw footprint polygon for the building can be derived by connecting all boundary points. However, the raw footprint is often noisy because of the irregularly spaced LIDAR measurements. It is a challenging task to derive an accurate footprint from a noisy and complex polygon. Alharthy and Bethel [15] employed a histogram of boundary points to generalize the footprint edges by assuming that the buildings have only two dominant directions that are perpendicular with each other. Based on the same assumption, Sampath and Shan [18] used the least squares model to regularize the footprint edges. However, this assumption is too strict and cannot be applied to buildings whose edges are not perpendicular to the dominant directions. It is not uncommon that both commercial and residential buildings have some segments that are not parallel to the dominant directions.

The main objective of this paper is to present a framework involving a series of algorithms for building footprint extraction from LIDAR measurements and an accuracy analysis for the proposed methods. The framework consists of three major steps. First, the non-ground and ground measurements are separated. Second, building measurements are identified by region growing using a local plane-fitting technique. Finally, footprints are derived and adjusted based on estimated dominant directions.

III. DERIVATION OF BUILDING FOOTPRINTS

A. Separating Ground and Non-Ground Measurements

Morgan and Tempfli [9] showed that classifying ground and non-ground measurements is a critical step for constructing building footprints. The ground and non-ground measurements are separated as a first step in the proposed framework using a progressive morphological filter [19]. We selected the progressive morphological filter because this filter identifies the ground and non-ground measurements well for the study areas which are located in a coastal urban setting with gentle slopes. Alternative filters can also be used in this step if those filters can produce a better classification.

Before filtering and building identification, a two-dimensional array was employed to represent points falling in cells of a mesh overlaying the data set to facilitate the computation. The cell size (c_s) of the mesh is usually set to be less than the average spacing of LIDAR points to reduce information loss. Each point measurement from the LIDAR data set is assigned to a cell in terms of its x and y coordinates. If more than one point falls in the same cell, the point with the lowest elevation is selected as the array element. If no point exists in a cell, the array element for the cell is assigned by its nearest neighbor. Since our main concern is to identify buildings, non-ground measurements whose heights are less than 2 m were removed to minimize the effect of trimmed bushes. The heights were derived by subtracting elevations interpolated using identified ground measurements from elevations of non-ground measurements.

B. Identifying Building Measurements

The second step of our method is to identify building measurements from non-building (mainly vegetation) data using the region growing algorithm based on a plane-fitting technique. Areas of connected non-ground measurements are found and labeled first by connecting the eight neighbors of a cell, recursively. For each non-ground measurement area, inside and boundary points are identified. If at least one of the eight neighbors of a point is a ground measurement, the point is defined as a boundary point. Otherwise, the point is an inside point.

Then, non-ground LIDAR measurements for each area are segmented by region growing based on a plane-fitting technique. Given an inside point $p_0(x_0, y_0, z_0)$, a Cartesian coordinate system (x, y, and z) is established using p_0 as the origin. In this coordinate system, a best fitting plane for p_0 and its eight neighbors is derived by using the least squares method. Assume that the plane is defined by:

$$z = ax + by + c \tag{1}$$

The parameters *(a, b, c)* can be derived by minimizing the sum of squares due to deviations (SSD)

$$min(SSD) = min \sum_{(p_k)\in M} (z_k - h_k)^2 \tag{2}$$

where M is a set for p_0 and its neighbors, and h_k and z_k are observed and plane fitted surface elevations, respectively.

Region growing segmentation starts with the selection of the seed point from the inside points for an area of connected non-ground measurements. The inside points for the area are sorted based on their SSDs in ascending order. The point with the minimum SSD is labeled and selected as the first seed point for region growing. The neighbors of a seed point are judged by whether they belong to the same category through a plane-fitting technique. A plane is constructed based on the points in the category using a least squares fit. The elevation from the candidate point to this plane is compared to a predefined threshold Δh_T to select the point. $\Delta h_T$is determined by the elevation error of the LIDAR survey and is usually 15-30 cm. If a neighbor is found to be in the same category, it is labeled and added to the category. The neighbors of the growing area are examined further, and the process is continued until no additional points can be added into the category. Next, the unlabeled inside points are sorted in terms of their SSDs, and region growing starts again from a labeled seed point with a

minimum SSD. The region-growing processes are repeated for each non-ground measurement area until all measurements are segmented.

After non-ground measurements are segmented, patches for non-building objects are removed by four steps. First, areas of patches are compared with a predefined area threshold *Min_Surface* (e.g. 5 m^2) to eliminate small and fragmented patches of vegetation. Second, eliminated small patches in the first step representing chimneys, water tanks, and pipe lines of buildings are recovered. The condition to include these small patches is they are completely surrounded by large patches. Third, isolated boundary points, none of whose eight neighbors is an inside point, are removed. Fourth, the remaining patches are merged in terms of their connectivity. Through this process, adjacent roof surfaces from the same building, having different slopes, are merged into a large building patch. Relatively large vegetation patches that are not removed in the first step remain in merged patches, however vegetation patch sizes are usually smaller compared to those of merged building roofs. Therefore, these vegetation patches are removed by comparing their area values to a threshold *Min_Building* that approximates the minimum area of a building, e.g. 60 m^2. The remaining patches after four operations are classified as building patches.

C. Deriving the Outline of a Building

With the building measurements identified, a raw footprint can be obtained by connecting the boundary points (Fig. 1a). However, the boundary of the raw footprint contains too many details and "zig-zag" noise because of the irregularly spaced point measurements and the grid based interpolation. In this section, the following three steps describe the method to reduce the noise of raw footprints.

1) Extracting the Coarse Footprint: Several algorithms have been employed to reduce the vertices of a noisy raw building footprint and derive a coarse footprint. Latecki and Lakamper [20] proposed a method based on a conspicuous value to remove boundary noise. The drawback of this method is that it is difficult to automatically define the termination condition. Weidner and Forstner [21] eliminated noisy vertices of a footprint polygon by comparing the heights of triangles formed by three consecutive vertices with a predefined threshold. The Douglas-Peucker algorithm [22] is another alternative to simplify lines with noise. The Douglas-Peucker algorithm generalizes lines by forming a line connecting start and end points first, and then recursively selecting a left point with a largest distance to the line until a predefined distance threshold *T_Douglas* is reached. The Douglas-Peucker algorithm was implemented in our framework because of its simplicity.

2) Estimating the Dominant Directions of a Building: The Douglas-Peucker algorithm occasionally removes critical corner vertices of a raw footprint due to the "zig-zag" pattern of boundary lines, thus distorting the orientation of segments and producing acute or obtuse angles between segments (Fig. 1b). In order to recover the removed critical vertices and distorted segments, the building footprints were divided into two categories. For the first category, there are two dominant directions for a building footprint polygon, and most segments

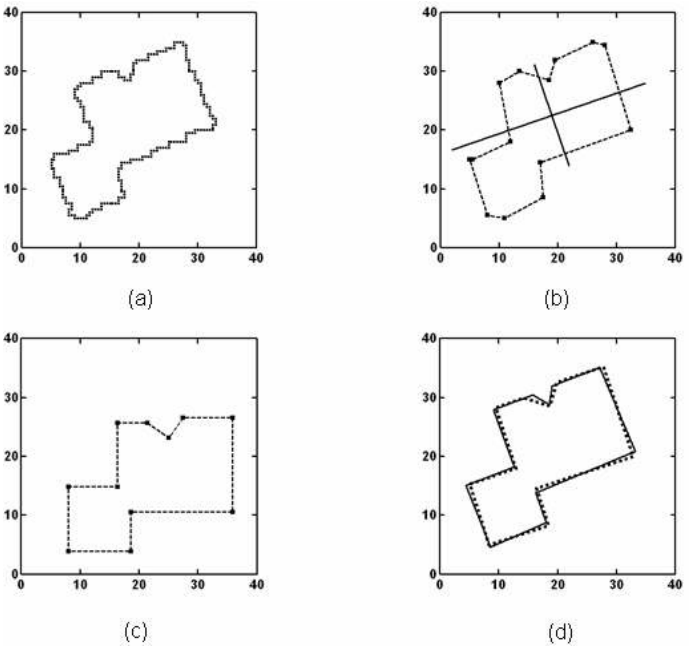

Fig. 1. Example to illustrate the framework for extracting building footprints. The x and y coordinate units are in meters. (a) The raw footprint derived by connecting boundary points of identified building measurements through the region growing algorithm. The raw footprint is noisy due to the interpolation of the irregularly spaced LIDAR measurements. (b) The coarse footprint (dash line) that was derived by applying the Douglas-Peucker algorithm to the raw footprint and the estimated dominant directions (solid line). (c) The adjusted footprint that recovered the critical corner vertices removed by the Douglas-Peucker algorithm. The footprint was rotated clockwise according to the estimated dominant directions. (d) Comparison of the final footprint (dot line) with corresponding known footprint (solid line).

are parallel or perpendicular to each other. For the second category, a considerable number of segments are oblique to the two dominant directions, or more than two dominant directions exist. The critical step in identifying these two categories of building footprints is to estimate the dominant directions.

Maas and Vosselman [23] derived dominant directions using invariant parameters, based on an assumption that the roof type of a building is already known. However, building roof types are not available in many cases before building footprints are identified [13]. Also, it is often difficult to classify the roofs of complex buildings into any given type. A 2D Hough Transform can be used to estimate the dominant directions of a building footprint. The major limitation of the Hough Transformation is that it is difficult to determine the optimum cell size in parameter space.

We have proposed a new method to estimate the dominant directions of a building footprint based on weighted line segment lengths. Let *x'* and *y'* represent possible dominant directions in a 2D coordinate system *x* and *y* (Fig. 2). The dominant directions *x'* and *y'* are related to the coordinate system *x* and *y* through a counterclockwise rotation by an angle $\varphi(0^0 \leq \varphi < 90^0))$. Therefore, the key step to estimate the dominant directions is to find the rotation angle φ. Assuming that the counterclockwise intersection angle between a line

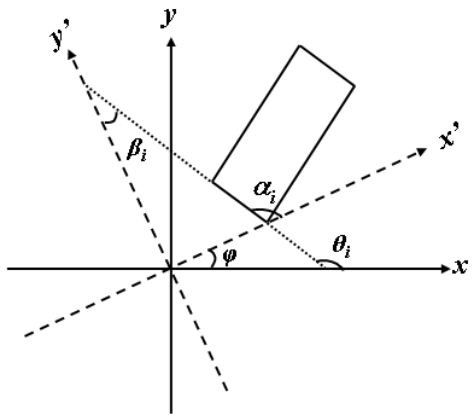

Fig. 2. Relationship between angles β_i, θ_i, α_i and φ. The coordinate system x' and y' is a counterclockwise rotation of the coordinate system x and y by an angle φ. θ_i is the counterclockwise intersection angle between a segment of a building footprint (solid square) and the axis x. α_i is the counterclockwise intersection angle between a segment and the axis x'. β_i is the minimum intersection angle between a segment and the axes x' and y'

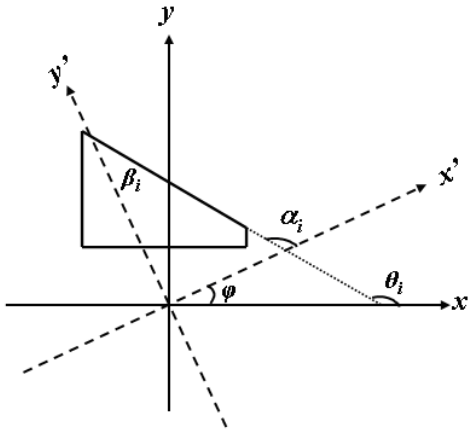

Fig. 3. A footprint with several parallel and perpendicular segments and an oblique line. The parallel and perpendicular segments align with dominate directions that are x and y axes. Angles β_i, θ_i, α_i and φ have the same definitions as those in Fig. 2.

segment and x axis is $\theta_i(0^0 \leq \theta_i < 180^0)$, we define

$$SL = \sum_{i=1}^{N} g(L_i) f(\beta_i(\theta_i, \varphi)) \tag{3}$$

where N is the total number of vertices of a building footprint, L_i is the segment length, $\beta_i(0^0 \leq \beta_i < 45^0)$ is the minimum intersection angle between a segment and the nearest axis in the coordinate system x' and y', and is determined by θ_i and φ. $g()$ is the weight function based on L_i, and $f()$ is the weight function based on and θ_i and φ. The dominant building directions can be estimated through finding an optimum φ so that SL will reach a minimum. A linear function is employed to represent $g()$

$$g(L_i) = L_i / \sum_{i=1}^{N} L_i \tag{4}$$

Finding the optimum φ depends heavily on $f()$ which can be in many forms such as linear and exponential. We would like to construct $f()$ such that the segments close to the dominant direction will have a small contribution to SL. Here a linear function is used to represent $f()$

$$f(\beta_i(\theta_i, \varphi)) = \beta_i / 45 \tag{5}$$

Obviously, the closer the segment is to the dominant direction, the smaller the $f()$. β_i is determined by

$$\beta_i = \begin{cases} min(\alpha_i, 90 - \alpha_i) & : \quad \alpha_i \leq 90 \\ min(180 - \alpha_i, \alpha_i - 90) & : \quad \alpha_i > 90 \end{cases} \tag{6}$$

where $\alpha_i(0^0 \leq \alpha_i < 180^0)$ is the counterclockwise intersection angle between a line segment and the axis x' and has the following relationship with θ_i and φ

$$\alpha_i = \begin{cases} \theta_i - \psi & : \quad \theta_i \geq \varphi \\ 180 + \theta_i - \varphi & : \quad \theta_i < \varphi \end{cases} \tag{7}$$

Numerically, the optimum φ is found by comparing SL values for angles between 0^0 and 90^0. After φ is derived, the building footprint is rotated so that the x and y axes are aligned with the dominant directions of the buildings.

Although the algorithm is simple, this method to estimate the dominant direction of a building is very robust and has the following property:

Estimated dominant directions are the same as the directions of parallel and perpendicular segments as long as the total length of oblique lines is less than the total length of parallel and perpendicular segments of a footprint.

Proof: Let directions for parallel and perpendicular segments be x and y, and possible dominant directions are x' and y' that are derived by rotating x and y axes with an angle φ (Fig. 3). Since θ_i is 180^0 (or 0^0) and 90^0 for parallel and perpendicular segments, respectively, β_i for parallel and perpendicular segments is the same (β_D) and equal to the rotation angle φ or the complementary angle of φ. Therefore, the contribution (SL_D) of rotated parallel and perpendicular segments to SL can be represented by

$$\begin{aligned} SL_D &= \sum_{i=1}^{N} g(L_i)\beta_i/45 \\ &= \beta_D L_D/45L_T \\ &= \begin{cases} \varphi L_D/45L_T & : \quad \varphi \leq 45 \\ (90-\varphi)L_D/45L_T & : \quad \varphi > 45 \end{cases} \end{aligned} \tag{8}$$

where L_D is the total length of parallel and perpendicular segments, and L_T is the total length of segments of a footprint. SL_D is a period function with minimum values at 0 and 90 and maximum value at 45 (Fig. 4). The amplitude and period of SL_D are L_D/L_T and 90, respectively.

The contribution (SL_O) of rotated oblique lines to SL can be described by

$$SL_O = \sum_{i=1}^{M} SL_{Oi} = \sum_{i=1}^{M} L_{Oi}\beta_{Oi}(\varphi, \theta_{Oi})/45L_T \tag{9}$$

where M is the number of oblique segments, SL_{Oi} is the contribution of *ith* oblique segment to SL, L_{Oi} is the length of *ith* oblique segment, and β_{Oi} is the minimum intersection

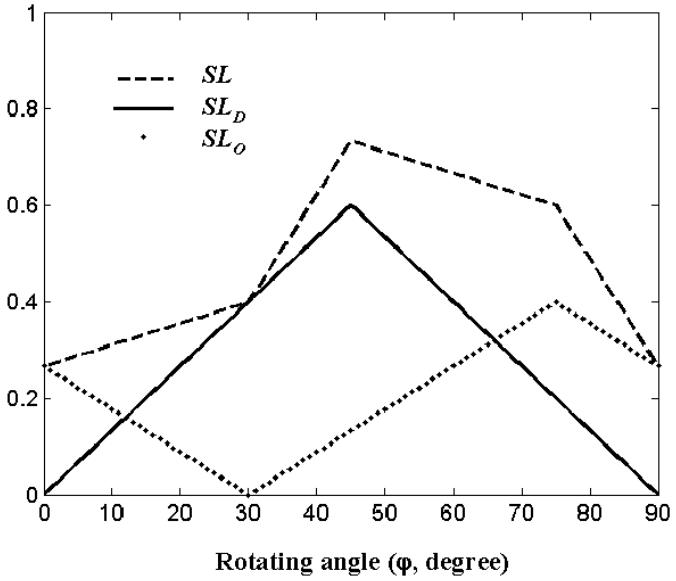

Fig. 4. SL_D, SL_O, and SL for a footprint with several parallel and perpendicular segments and an oblique line. The length of parallel and perpendicular segments is 60% of the total length of segments, and the length of the oblique line is 40% of the total length of segments. The θ_O for the oblique line is 120^0. The directions of parallel and perpendicular segments are the dominant directions of the footprint.

angle between the oblique segment and the nearest axis in the coordinate system *x'* and *y'*. Similar to SL_D, SL_{Oi} has period of 90 and amplitude of L_{Oi}/L_T. The initial phase of SL_{Oi} is determined by the counterclockwise intersection angle θ_{Oi} between the oblique segment and *x* axis. Fig. 4 shows the change of SL_{Oi} as a function of φ when θ_{Oi} is 120^0.

In order to facilitate the analysis, we divided SL into two sections: $\varphi < 45^0$ and $\varphi > 45^0$ In section $\varphi < 45^0$, SL becomes

$$SL = \varphi L_D/45L_T - \sum_{i=1}^{M} L_{Oi}\beta_{Oi}(\varphi, \theta_{Oi})/45L_T \qquad (10)$$

The derivative of SL with respect to φ is

$$\frac{\partial SL}{\partial \varphi} = \frac{1}{45L_T}(L_D + \sum_{i=1}^{M} \pm L_{Oi}) > \frac{1}{45L_T}(L_D - L_O) \quad (11)$$

where L_O is the total length of oblique segments. The sign before L_{Oi} is determined by θ_{Oi} and φ. Since $L_D > L_O$, no matter how SL_O changes, SL, like SL_D, increases monotonically in section $\varphi < 45^0$. Similarly, we can demonstrate that SL decreases monotonically in section $\varphi > 45^0$. This indicates that SL reaches minimum at $\varphi = 0$ or $\varphi = 90$. There are no better dominant directions for the footprint other than the directions of parallel and perpendicular segments as long as the total length of parallel and perpendicular segments is larger than that of oblique lines. ■

3) Adjusting the Footprint: For the first category of building footprints which have two distinct dominant directions, a unique optimum φ can be derived. The SL value for a rotated footprint should be small. However, for the second category of building footprints, multiple optimum φ could be derived. In such a case, the first optimum φ is used to rotate the footprint. The SL value for the second category of footprints should be large. Therefore, the SL value for each rotated building footprint was employed to classify the footprint. If the SL value is less than a threshold T_SL (e.g., 0.3), the footprint is classified as the first category which has two dominant directions. Otherwise, the footprint belongs to the second category. For the first category, we propose an algorithm to recover the critical vertices based on two assumptions:

- Each building has two dominant directions and they are perpendicular to each other
- Most (e.g., 80%-90%) of the boundary segments are parallel to one of the two dominant directions

Segments of the rotated footprint are adjusted using four types of operations. The ***split*** operation is used to adjust certain horizontally and vertically oblique segments. The adjustable horizontally oblique segment is the line whose projection on the *x* axis is equal to or greater than the *y* axis, and whose projection on the *y* axis is less than a threshold $T\_Projection$. The adjustable vertically oblique segment is the line whose projection on the *x* axis is less than the *y* axis, and whose projection on the *x* axis is less than $T\_Projection$. Fig. 5a shows how an adjustable horizontally oblique segment P_1P_2 is straightened by adding two more points $P_3^{'}$ and $P_4^{'}$ using ***split***. Line P_1P_2 is replaced by three lines $P_1P_3^{'}$, $P_3^{'}P_4^{'}$, $P_4^{'}P_2$, among which $P_3^{'}P_4{'}$ is horizontal. The *x* coordinates of vertices $P_3^{'}$ and $P_4^{'}$ are the same as those of P_1 and P_2. The *y* coordinates are the average of P_1 and P_2, respectively. A similar operation can be applied to an adjustable vertically oblique segment by exchanging the *x* and *y* coordinates.

The ***intersect*** operation is employed to recover the missing corner as shown in Fig. 5b. This operation compares the ratio *R* of the area of the triangle P_2PP_3 to that of triangle P_1PP_4. If the *R* is less than the threshold T_Ratio, the four points P_1, P_2, P_3, and P_4 are replaced with points P_1, P and P_4.

The ***merge*** operation adjusts four consecutive points P_1, P_2, P_3, and P_4 when P_1P_2 is parallel to P_3P_4, but not collinear. Without loss of generality, P_1P_2 is assumed to be horizontal. The operation can be applied to the case when P_1P_2 is vertical by exchanging the *x* and *y* coordinates. There are three types of merge operations. The first type is for the case that P_1P_2 is opposite to P_3P_4 (Fig. 5c). If the distance between P_1P_2 and P_3P_4 is less than the threshold $T\_Deviation$, the merge operation replaces the four original points with P_1, P and P_4. This operation is used to remove the long, thin portion protruding from a footprint. For the other two types of merge operations, P_1P_2 has the same direction as that of P_3P_4. The difference is that the projection of line P_1P_4 on the *x* axis is longer than that on the *y* axis for the second type (Fig. 5d), while the projection on the *x* axis is shorter for the third type (Fig. 5e).

A horizontal segment $P_2^{'}P_3^{'}$ is constructed for the second type of merge so that $P_1P_2^{'}$ and $P_3^{'}P_4$ are vertical. The *y* coordinates of $P_2^{'}$ and $P_3^{'}$ are between those of P_1 and P_4 and

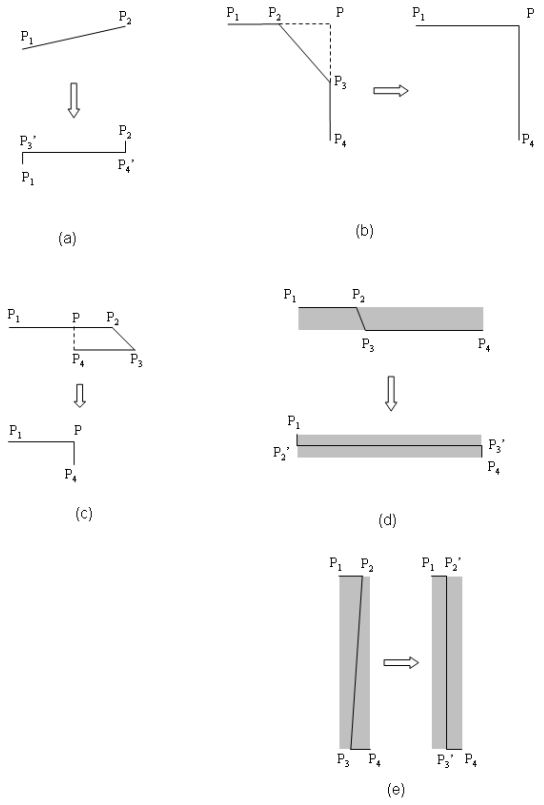

Fig. 5. Operations proposed to adjust segments of a footprint (a) ***split***, (b) ***intersect***, (c) first type of ***merge***, (d) second type of ***merge***, and (e) third type of ***merge***.

are inversely proportional to lengths $L_{P_1P_2}$and$L_{P_3P_4}$

$$y = y_3 + (y_2 - y_3)\frac{L_{P_1P_2}}{L_{P_1P_2} + L_{P_3P_4}} \tag{12}$$

where y_2 and y_3 are coordinates of P_2 and P_3 on the y axis. If the difference $|y_2 - y_3|$ is less than the threshold $T\_Deviation$, the original four consecutive points P_1, P_2, P_3, and P_4 are converted into P_1, $P_2^{'}$, $P_3^{'}$ and P_4 by the ***merge*** operation. The third type of merge operation is illustrated in Fig. 5e. A vertical $P_2^{'}P_3^{'}$ is constructed by using the average of x coordinates of P_2 and P_3 and y coordinate of P_2 or P_3. If the absolute difference between y coordinates of P_2 and P_3 is less than threshold $T\_Deviation$, the points P_1, P_2, P_3, and P_4 are replaced by P_1, $P_2^{'}$, $P_3^{'}$ and P_4.

The ***remove*** operation is designed to remove the redundant vertices of a line. Extra vertices may exist on a segment of the footprint after operations ***split***, ***intersect***, and ***merge*** are performed. These extra collinear vertices are eliminated using the remove operation immediately after performing one of three other operations.

The segments of the first category of building footprints are adjusted iteratively using the four operations starting from a small value of $T\_Projection$. $T\_Projection$ is incremented gradually until the percentage of the lengths of horizontal and vertical segments of a footprint is over the predefined threshold $T\_Footprint$. $T\_Footprint$ is usually set to be between 80% and 90% of the perimeter of the adjusted footprint. Fig. 1c displays a building footprint refined from the coarse footprint (Fig. 1b). Corner vertices lost due to the line simplification by the Douglas-Peucker algorithm were recovered successfully by our footprint adjustment algorithm.

The same operations and procedure are employed to adjust the second category of building footprints. However, it is not appropriate to use the threshold $T\_Footprint$ as a termination condition because a considerable number of segments are not parallel to the estimated dominant directions. A footprint could be distorted severely if a large $T\_Footprint$ is used. Therefore, an alternative termination condition for footprint adjustment is employed. The iteration is stopped when $T\_Projection$ is greater than a threshold $T\_Projection\_Final$ to avoid adjusting long oblique segments.

IV. DATA PROCESSING

The study area is located at and around the campus of Florida International University (FIU), covering 6 km^2 of low relief topography. Surveyed features include residential houses, complex buildings, individual trees, forest stands, parking lots, open ground, ponds, roads, and canals. The data were collected in April 2000 and August 2003 with Optech ALTM 1210 and 1233 systems operated by FIU, respectively. The Optech system recorded the coordinates (x, y, z) and intensity of the point measurements corresponding to first and last laser returns. The 2000 data set consists of three overlapping, 400 m wide swaths of 15 cm diameter footprints spaced approximately 2 m apart. The 2003 data set consists of five overlapping, 340 m wide swaths of 13 cm diameter footprints spaced approximately 1 m apart.

Building footprints were extracted from two test LIDAR data sets for the FIU campus and adjacent areas to examine their effectiveness. The thresholds used in our experiments for the FIU campus dataset are listed in Table I. These thresholds were derived empirically by visually comparing the results with gridded raw LIDAR measurements. This is feasible because it took 9, 2, and 0.7 minutes for a PC with 2.8 GHz processor and 2 GB RAM to perform morphological filtering, building measurement identification, and footprint derivation for the FIU campus dataset. A two dimensional array with about 7.2 million elements was employed to represent raw and interpolated points covering an area of 1.8 km^2. Sensitivity analysis showed that small changes in these thresholds have little impact on the final results.

Aerial photographs, a building footprint map from the FIU Planning and Facility Management Department, and field investigation were used to qualitatively and quantitatively evaluate the derived footprints. The aerial photographs were collected in 1999 at a resolution of 0.3 m. The Planning and Management Department footprint map was made mainly through ground surveying when buildings were constructed and included 62 buildings. All surveyed buildings can be found on the aerial photographs and they did not change over the time. Therefore, these buildings can be used to quantify errors introduced by our framework.

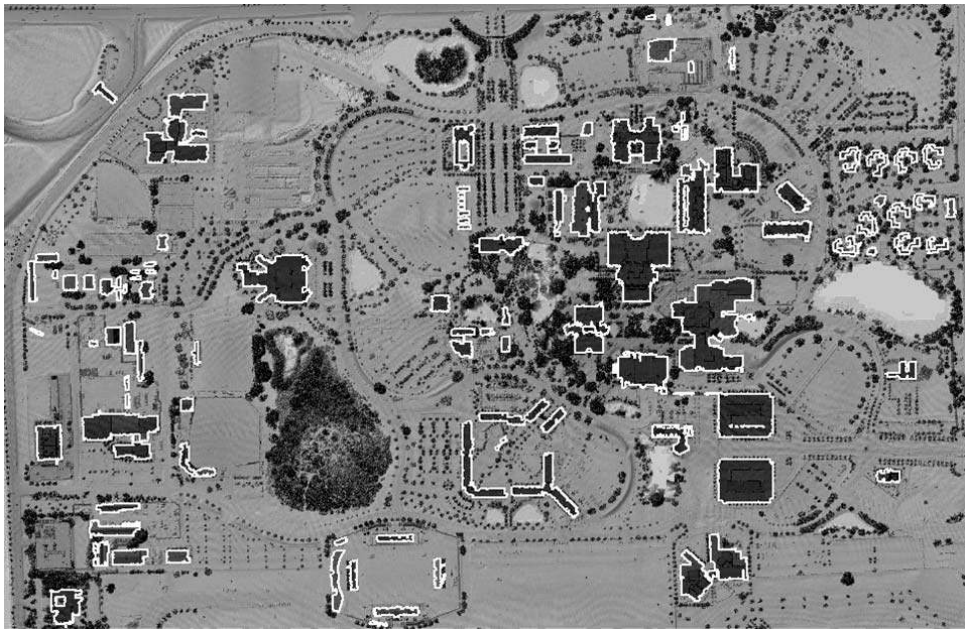

Fig. 6. The raw footprints for buildings at FIU Campus. Raw footprints were derived by connecting boundary points of identified building measurements using the region growing algorithm. The background image was derived by interpolating raw LIDAR point measurements.

TABLE I
PARAMETERS FOR EXTRACTING SIMPLE BUILDING MODELS

Cell size (c_s) for progressive morphological filter	0.5 m
Height difference to aggregate a point (Δh_T)	0.2 m
Minimal surface on the roof ($Min\_Surface$)	5 m^2 (20 c_s^2)
Minimal building area ($Min\_Building$)	60 m^2 (240 c_s^2)
Douglas distance ($T\_Douglas$)	1.5 m (3 c_s)
Threshold for footprint classification (T_SL)	0.3
Threshold for split adjustment ($T\_Projection\_Final$)	2 m (4 c_s)
Threshold for deviation ($T\_Deviation$)	2 m (4 c_s)
Threshold for triangle area ratio (T_Ratio)	0.1
Threshold for footprint evaluation ($T\_Footprint$)	0.85

V. RESULTS

Both qualitative and quantitative methods were employed to measure the errors committed in extracting building footprints in this study. A qualitative method checks the quality of estimated dominant directions and derived footprints by visually comparing the extracted footprints with those in maps and aerial photographs. The quantitative method examines the accuracy by extending the count-based metric method proposed by Shufelt and Mckeown [3] and area-based metric method suggested by Ruther et al. [4]. The count-based metric method quantifies commission and omission errors in the number of buildings identified. The area-based metric method measures the changes of two footprints derived from different stages of the proposed framework. Raw footprints derived by connecting boundary points from identified building measurements are placed over known building footprints to examine the accuracy of the region growing segmentation algorithm. The omission error is measured by the percentage of area not in the raw footprint but in the known building footprints. The commission error is measured by the percentage of area in the raw footprint but not in the known building data set. Raw and adjusted footprints are compared to evaluate the changes induced by the vertex recovery algorithm. The commission and omission errors from comparison of final building footprints with corresponding known building footprints are employed to measure the performance of the entire framework.

To demonstrate the effectiveness of the proposed framework for building footprint extraction, the results from last return measurements of the 2003 data set are presented in detail in this section. Fig. 6 displays raw footprints for identified building areas at the FIU campus. Count-based error analysis shows that all buildings were identified and no tree areas were mistakenly included. Area-based error analysis compared raw footprints with known building footprints. The results show that omission and commission errors are 10% and 2%, respectively, indicating that the segmentation algorithm worked well to identify most building measurements. The commission error occurs because the elevation change of some trees adjacent to buildings is similar to those of buildings (Fig. 7a). These tree measurements were mistakenly included by the region growing segmentation. The omission errors are 6 percent larger than commission errors. The major reason for the relatively large omission error is that there are 40 buildings whose areas are larger than 600 m^2 in the known building footprint data set. Most roofs of the large buildings are flat with narrow high surfaces at edges. These edges are often removed by plan-fitting technique because of large elevation deviations. Another factor is the trees covering roofs that prevent the portion of buildings underneath the trees from being identified (Fig. 7b).

The effect of the footprint adjustment algorithm is well illustrated in Fig. 8. Fig. 8a shows that the raw building footprints have noise on their boundaries. Most of the noise was removed in the adjusted footprints as shown in Fig. 8b and the smoothness of the footprint polygons was greatly improved. To test the deviation caused by the footprint adjustment algorithm,

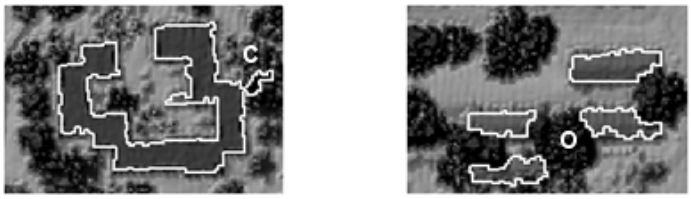

Fig. 7. Examples of errors caused by the region growing building segmentation algorithm. (a) Commission error (**C**): the flat tree top next to the building is misidentified as a part of the building. (b) Omission error (**O**): the corner portions of buildings were missed because the roofs are partially covered by trees.

raw footprints were compared with adjusted footprints. The results show that the deviation is small. About 3% of the raw footprints are not contained in adjusted footprints, and 3% of the footprints are mistakenly added to the adjusted footprints. By visually comparing the adjusted footprints with raw footprints, we found that in most cases the adjusted footprints preserve the original geometric shape.

The effectiveness of the algorithm to estimate dominant directions was evaluated by visually examining all final footprints. The algorithm worked well for all buildings at the FIU campus. For example, Fig. 9a shows a complex building which consists of five major parts. The dominant directions were estimated to be nearly horizontal in terms of three major rectangles. A circle portion (C in Fig. 9a) was approximated by several line segments (Fig. 9b). A small oblique rectangle (R in Fig. 9a) whose direction is different from the dominant directions was also adjusted appropriately.

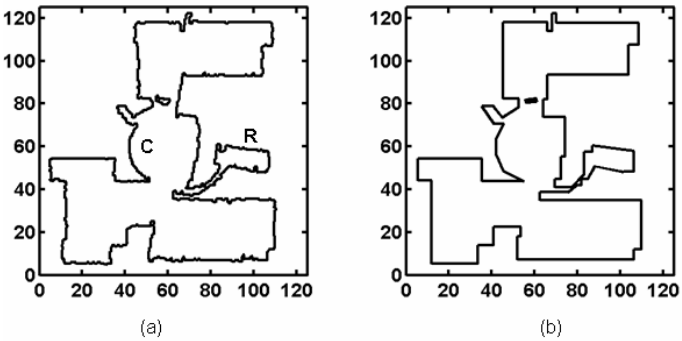

Fig. 9. The raw (a) and final (b) footprint for a complex building. The x and y coordinate units are meters. Two dominant directions of the footprint are nearly horizontal and vertical. Note that the arc of a circle (C in a) of the footprint is approximated by a polyline. A small rectangle (R in a) that is not aligned with the dominant directions is well preserved.

Fig. 10 shows a 3D building map for FIU campus based on final building footprints and heights. The heights of the buildings were derived by averaging the elevation differences between building measurements and the digital terrain model (DTM) interpolated from ground measurements. These building models have been used to construct a 3D synthetic visual environment to animate hurricane-induced fresh water flooding at FIU campus. Comparison of 62 final footprints with footprints from the map provided by the FIU Planning and Facility Management Department shows that 10% of the building footprints were mistakenly removed, and 2% of the footprints were incorrectly included into the final output by our framework. Both the omission and commission errors for the final footprints are almost the same as those caused by the region growing segmentation algorithm. This further proves that the deviations caused by the footprint adjustment algorithm have little effect on the final result. Therefore, the errors in final footprints mainly come from the errors before the footprint adjustment is performed.

Building extraction results for a residential area are displayed in Fig. 11. The known building footprint data for the residential area were derived by digitizing buildings from aerial photographs. The relief displacement of the residential houses in the orthorectified photograph was small due to their low heights. The digitized footprints were overlaid over a grid interpolated from raw LIDAR measurements to ensure quality. The data set included 211 building footprints, and the parameters used by the framework are the same as those listed in TABLE I. All buildings were identified from LIDAR data and there were no commission and omission errors from the count-based accuracy analysis. Both area-based omission and commission errors for final footprints were about 6%, indicating that the framework worked well in residential areas.

Several factors influence the accuracy of building measurement identification. One of them is the point measurement used in computation. Most airborne LIDAR systems are capable of deriving first and last return measurements for an emitted laser pulse. Both first and last return measurements can be used to identify the building footprints. However, there are different advantages and disadvantages in using them. The first return measurements suffer fewer errors from multipath reflections which can be caused by many factors. For example, when a laser pulse hits glass walls or windows, it can enter the room and bounce several times before it finally reaches the sensor. The multipath reflection of a laser pulse can lead to incorrect low elevation measurements for the roof of a building. These low elevation points are often removed as ground measurements by the progressive morphological filter, resulting in small holes in the building footprint. There are many more multipath errors in the last return measurements than in the first return measurements in our data set. However, the last return measurements have more of a chance to penetrate into the vegetation and reach the ground. This helps the filter to separate the ground and non-ground measurements. Also, the last return measurements display more spatial change than the first return in tree areas, which helps separate the building measurements from tree measurements. The current building identification methods have been applied to both first and last return data in the study area. It was found that the last return measurements have a better overall performance. Improvement of the current algorithms by combining the first and last return measurements need to be further investigated.

The performance of the region growing algorithm to segment building measurements in the proposed framework is critical to the footprint extraction. The processes of region growing segmentation rely on the selection of seed points. In our algorithm, the seed points are selected in terms of minimum SSDs based on a plane-fitting technique. To examine the robustness of the algorithm, other methods for selecting

Fig. 8. Comparison of raw (a) and adjusted (b) building footprints. The small "zig-zag" noise in the raw footprints were removed in the adjusted footprints, making the adjusted footprints look more realistic.

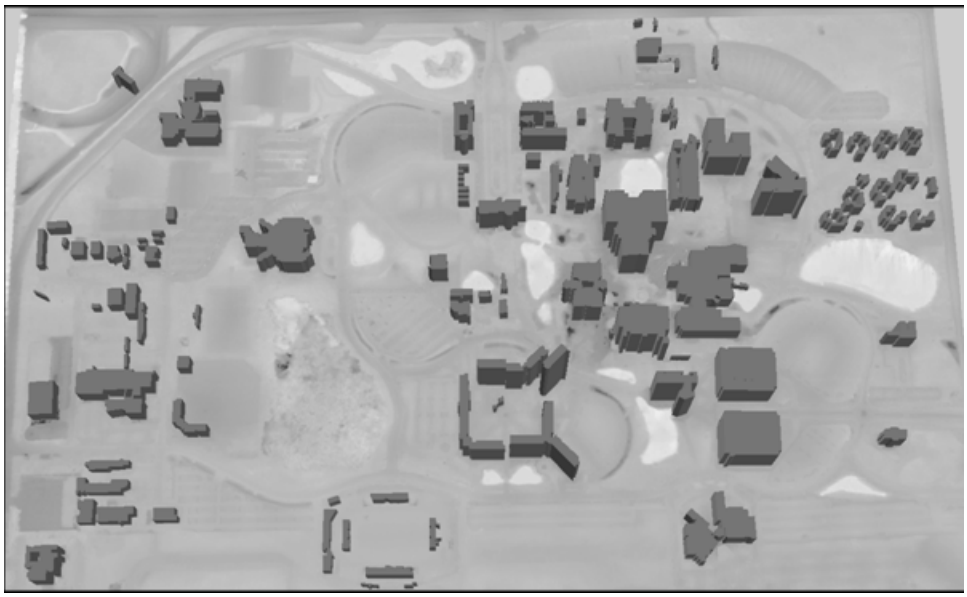

Fig. 10. 3D building models for FIU campus. Each building model was created using the final footprint and average building height derived from LIDAR measurements. The DTM for building bases was derived by interpolating ground measurements identified by the progressive morphological filter.

seed points were tested for the FIU campus data set. One alternative method is to start seed point selection at the left upper corner of a non-ground area, and then select seed points based on an increased order of x coordinates and a decreased order of y coordinates. Comparison of the seed point selection starting at the left upper corner with that based on minimum SSDs shows that slight differences sometimes occur in areas of individual patches (roof surfaces) within a building footprint, especially for those points at the boundaries between two roof surfaces. However, there is little difference between the identified measurements for the whole building when individual patches are merged for the building.

Three other cases with different combinations of increased or decreased x and y coordinates have also been tested. The results show that the maximum difference between identified building measurements using these combinations and those from minimum SSDs is less than 1%. A random selection of seed points was also performed for individual building areas, and the results also show that the selection of seed points has little impact on the building measurement identification. This indicates that the region growing algorithm based on plane-fitting is robust for segmenting building measurements.

LIDAR measurement density also has great effect on segmentation results. The LIDAR points for 2000 and 2003 data sets are spaced approximately 2 m and 1 m, respectively. To test the effect of point density, building footprints were extracted from both data sets. Comparison of the footprints for the same buildings shows that the 2003 data set with a higher point density produced a much better result for the FIU Campus because small building surfaces removed in the 2000 data set were preserved in the 2003 data set. The total of commission and omission errors of final footprints for the 2000 data set was about 17%, a 5% increase compared to a total error of 12% for the 2003 data set (TABLE II). The effect of point density on the residential area is more substantial as the total area-based error increases to 35%. This large error is mainly due to the fact that residential buildings are small and 2000 LIDAR measurements are not dense enough to capture

Fig. 11. Building footprints extracted from LIDAR data for a residential area.

TABLE II

ERROR ANALYSIS RESULTS FOR TWO DATASETS COVERING THE FIU CAMPUS AND A RESIDENTIAL AREA. THE KNOWN BUILDING FOOTPRINTS WERE PROVIDED BY THE FIU PLANNING AND FACILITY MANAGEMENT DEPARTMENT AND INCLUDE 62 BUILDINGS. THE KNOWN BUILDING FOOTPRINT DATA FOR THE RESIDENTIAL AREA INCLUDE 211 BUILDINGS AND WERE DERIVED BY DIGITIZING BUILDINGS ON AERIAL PHOTOGRAPHS AND AN IMAGE INTERPOLATED FROM RAW LIDAR MEASUREMENTS.

Omission Error	FIU Campus (2003)	FIU Campus (2000)	Residential (2003)	Residential (2000)
Raw footprint $vs.$ Known footprint	10.4%	17.1%	6.6%	30.3%
Raw footprint $vs.$ adjusted footprint	3.0%	3.1%	4.8%	8.4%
Adjusted footprint $vs.$ Known footprint	10.4%	17.2%	6.0%	30.6%
Commission Error	**FIU Campus (2003)**	**FIU Campus (2000)**	**Residential (2003)**	**Residential (2000)**
Raw footprint $vs.$ Known footprint	1.8%	1.4%	6.0%	5.3%
Raw footprint $vs.$ adjusted footprint	3.2%	3.2%	4.9%	7.5%
Adjusted footprint $vs.$ Known footprint	1.9%	1.4%	5.5%	4.8%

the boundary of the buildings.

VI. CONCLUSION

A framework including a series of algorithms has been developed to extract a building footprint from LIDAR measurements. The framework includes three major components: (1) the progressive morphological filter for separating the ground and non-ground measurements, (2) a region growing algorithm based on a local plane-fitting technique for segmenting building measurements, and (3) the Douglas-Peucker algorithm for removing noise in a footprint, an algorithm for estimating the dominant direction of a building, and an algorithm for adjusting the footprint based on estimated dominant directions. The entire process is highly automatic and requires little human aid, which is very useful for processing voluminous LIDAR measurements.

The novel algorithm for direction estimation is capable of identifying dominant directions as long as the total length of parallel and perpendicular segments is larger than the total length of oblique segments in a footprint. The allowance of oblique segments in a footprint enables users to perform footprint refinement for complex buildings in urban environments. The algorithms for dominant direction estimation and footprint adjustment can also be applied to generalize noisy raw building footprints derived from aerial photographs and high-resolution satellite images.

Application of the framework to the FIU campus and a residential area shows that the algorithms identified building measurements from LIDAR data and extracted footprints effectively. The quantitative accuracy analysis indicates that all buildings were identified and about 12% of the area errors were committed by the proposed algorithms, despite the fact that there are several complex building shapes on the FIU campus. These results provide a good basis for refining the footprint manually in a GIS environment for engineering applications which need highly accurate footprint information.

The point density of LIDAR measurements influence the accuracy of building footprint extraction, and approximately 1 m spaced LIDAR points are needed to achieve the above accuracy. The region growing segmentation algorithm for

identifying building points from non-ground measurements is critical for building footprint extraction. Experiments demonstrated that region growing segmentation based on local plane-fitting is robust and not sensitive to seed point selection.

ACKNOWLEGMENT

The authors would like to thank anonymous reviewers for valuable comments.

REFERENCES

[1] J. R. Jensen, *Remote Sensing of the Environment*. Upper Saddle River, NJ:Prentice Hall, 2000.

[2] Dewberry Davis, "Evaluation of alternatives in obtaining structural elevation data," *Federal Emergency Management Agency Report* ($http://www.fema.gov/nfip/alt\_elevations.shtm$), 2005

[3] J. A. Shufelt and D. M. Mckeown, "Fusion of monocular cues to detect man-made structures in aerial imagery," *Computer Vision Graphics and Image Understanding*, vol. 57, pp. 307-330, 1993.

[4] H. Ruther, H. M. Martine, and E. G. Mtalo, "Application of snakes and dynamic programming optimization technique in modeling of buildings in informal settlement areas," *ISPRS Journal of Photogrammetry and Remote Sensing*, vol. 56, pp. 269-282, 2002.

[5] A. Strassopolou, T. Caelli, and R. Ramirez, "Automatic extraction of building statistics from digital orthographs," *International Journal of Geographic Information System Science*, vol. 14, pp. 759-814, 2000.

[6] D. S. Lee, J. Shan, J. S. Bethel, "Class-guided building extraction from Ikonos imagery," *Photogrammetric Engineering and Remote Sensing*, vol. 69, pp.143-150, 2003.

[7] H. G. Maas, "Fast determination of parametric house models from dense airborne laser scanner data," in *ISPRS workshop on mobile mapping technology*, vol.32, Part 2W1, 5W1, IC5/3W, Bangkok, Thailand, 1999.

[8] S. Filin, "Surface clustering from airborne laser scanning data," in *ISPRS Commission III Symposium, Photogrammetric and Computer Vision*, Graz, Austria, pp. 119-124, 2002.

[9] M. Morgan and K. Tempfli, "Automatic building extraction from airborne laser scanning data," in *Proceeding of the 19th ISPRS Congress*, Book 3B, Amsterdam, Netherlands, pp. 616-623, 2000.

[10] F. Rottensteiner and J. Jansa, "Automatic extraction of buildings from LIDAR data and aerial images," in *International Archives of Photogrammetry and Remote Sensing*, vol. XXXIV, Part IX, pp. 569-574, 2002.

[11] A. F. Elaksher, J. S. Bethel, "Reconstructing 3D Buildings from LIDAR Data," in *ISPRS Commission III Symposium, Photogrammetric and Computer Vision*, Graz, Austria, pp. A 102-107, 2002.

[12] G. Sithole and G. Vosselman, "Experimental comparison of filter algorithms for bare-earth extraction from airborne laser scanning point clouds." *ISPRS Journal of Photogrammetry and Remote Sensing*, Vol. 59, pp. 85-101, 2004.

[13] M. Morgan and A. Habib, "Interpolation of LIDAR data and automatic building extraction," in *ACSM-ASPRS 2002 Annual Conference Proceedings*, 2002.

[14] S. O. Elberink and H. G. Maas, "The use of anisotropic height texture measures for the segmentation of airborne laser scanner data," in *International Archive of Photogrammetry Remote Sensing*, vol. XXXIII, Part B3/2, pp. 678-684, 2000.

[15] A. Alharthy and J. Bethel, "Heuristic filtering and 3D feature extraction from LIDAR data", in *ISPRS Commission III Symposium, Photogrammetric and Computer Vision*, Graz, pp. A 29-34, 2002.

[16] G. Vosselman, "Building reconstruction using planar faces in very high density height data," in *International Archive of Photogrammetry Remote Sensing*, vol. XXXIV, Part 3/W4, pp. 211-218, 2001.

[17] J. Overby, L. Bodum, E. Kjems, and P. M. Ilse, "Automatic 3D building reconstruction from airborne laser scanning and cadastral data using Hough transform," in *Proceeding of the ISPRS 20th congress - commission III*, Istanbul, Turkey, 2004.

[18] A. Sampath and J. Shan, "Urban modeling based on segmentation and regularization of airborne lidar point clouds," in *Proceeding of the ISPRS 20th congress - commission III*, Istanbul, Turkey, 2004.

[19] K. Zhang, S-C. Chen, D. Whitman, M-L. Shyu, J. Yan and C. Zhang, "A progressive morphological filter for removing non-ground measurements from airborne LIDAR data," *IEEE Transactions on Geoscience and Remote Sensing*, vol. 41, pp. 872-882, 2003.

[20] L. J. Latecki and R. Lakamper, "Convexity rule for shape decomposition based on discrete contour evolution," *Computer Vision and Image Understanding*, vol. 73, pp. 441-454, 1999.

[21] U. Weidner and W. Forstner, "Towards automatic building reconstruction from high resolution digital elevation models," *ISPRS Journal of Photogrammetry Remote Sensing*, vol. 50, pp. 38-49, 1995.

[22] D.H. Douglas and T. K. Peucker, "Algorithms for the reduction of the number of points required to represent a digitized line or its caricature," *The Canadian Cartographer*, vol. 10, pp. 112 -122, 1973.

[23] H. G. Maas and G. Vosselman, "Two algorithms for extracting building models from raw laser altimetry data," *ISPRS Journal of Photogrammetry and Remote Sensing*, vol. 54, pp. 153-163, 1999.

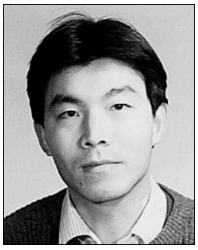

Keqi Zhang received the Ph.D. degree from the Department of Geography, University of Maryland, College Park, 1998. Since 1999, he has been a Research Assistant Professor in the International Hurricane Center, Florida International University, Miami. His research interests include airborne LIDAR mapping, 3D Visualization and GIS. He has authored and coauthored more than 20 papers in journals. Currently, he is leading a team to develop the high-resolution storm surge model and 3D visualization of storm surge flooding.

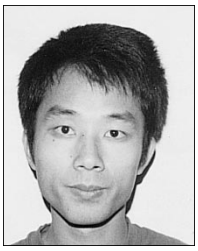

Jianhua Yan received the M.S. degree from the Institute of Image Processing and Pattern Recognition, Shanghai Jiaotong University, Shanghai, China, in 2000. He is currently pursuing the Ph.D. degree at the School of Computer Science, Florida International University, Miami. His research interests include image processing, pattern recognition, GIS, spatial database and neural networks.

Shu-Ching Chen (M'95-SM'04) received his Ph.D. from the School of Electrical and Computer Engineering at Purdue University, West Lafayette, IN, USA in December, 1998. He also received Master.s degrees in Computer Science, Electrical Engineering, and Civil Engineering from Purdue University. He has been an Associate Professor in the School of Computing and Information Sciences (SCIS), Florida International University (FIU) since August, 2004. Prior to that, he was an Assistant Professor in SCIS at FIU dating from August, 1999. His main research interests include distributed multimedia database systems and multimedia data mining. Dr. Chen has authored and co-authored more than 140 research papers in journals, refereed conference/symposium/workshop proceedings, and book chapters. In 2005, he was awarded the IEEE Systems, Man, and Cybernetics Society's Outstanding Contribution Award. He was also awarded a University Outstanding Faculty Research Award from FIU in 2004, Outstanding Faculty Service Award from SCIS in 2004 and Outstanding Faculty Research Award from SCIS in 2002.